Available online at www.sciencedirect.com
SCIENCE DIRECT®
Computers and Structures 83 (2005) 181–189
Computers & Structures
www.elsevier.com/locate/compstruc

Fluid–structural interactions in the inner ear

M. Kassemi [a,*], D. Deserranno [b], J.G. Oas [c]

[a] National Center for Microgravity Research, MS 110-1, NASA Glenn Research Center, 21000 Brook Park Rd, Cleveland, OH 44135, USA
[b] Department of Biomedical Engineering, Case Western Reserve University, Cleveland, OH 44106, USA
[c] Department of Otolaryngology, Cleveland Clinic Foundation, Cleveland, OH 44195, USA

Accepted 17 August 2004
Available online 11 November 2004

Abstract

This paper presents a finite element fluid–structural interaction model for the lateral semicircular canal system of the inner ear. The endolymph is modeled as a slightly compressible Newtonian fluid and the cupula partition is represented by a linearly elastic solid. The fluid–structural interaction problem is treated rigorously with a strong coupling between the fluid flow and the structural displacements. The time evolution of the endolymphatic velocity and pressure fields and cupular displacement and stress fields are closely examined to reveal the intricate dynamics that takes place in the vestibular system during the caloric irrigation test.

Keywords: Caloric test; CFD; Fluid structural interaction; Inner ear; Vestibular system

1. Introduction

The internal ear is a triumph of miniaturization and optimization; a three-dimensional inertial-guidance system, an acoustic amplifier and a frequency analyzer all compacted into the volume of a child's marble. The reliable and efficient performance of the inner ear depends on a magnificent complement of hydraulic and mechano-electrical transduction processes that are responsible in the cochlea for our sensitivity to sound, in the utricule and saccule for our perception of linear acceleration and gravity, and in the three semicircular canals (SCC) for our appreciation of rotary acceleration. In this paper, we are concerned with the fluid–structural dynamics that takes place in the semicircular canals of the vestibular system. When the head is subject to an angular acceleration the lag in the endolymphatic fluid in the SCC imparts a force on a sail-like membrane called the cupula. The cupula partition is embedded with sensory hair cells. As the cupula deforms, an intricate transduction process involving the hair cells generates signals which when processed by the brain determine the magnitude and direction of the imposed angular acceleration. This information is automatically coordinated with the eyes thus enabling the maintenance of gaze during a head movement. Naturally, any alteration of this intricate and synergetic fluid–structural interaction (FSI) by disease or by environment would result

* Corresponding author. Tel.: +1 216 433 5031; fax: +1 216 433 5033.
E-mail address: mohammad.kassemi@grc.nasa.gov (M. Kassemi).

0045-7949/$ - see front matter © 2004 Elsevier Ltd. All rights reserved.
doi:10.1016/j.compstruc.2004.08.001

in vestibular disorders with symptoms such as vertigo, and dizziness.

One of the most widely used non-physiological techniques for examining vestibular performance is the caloric stimulation test. This procedure uses thermal irrigation of the ear canal with cold and/or hot fluid (water or air) to elicit a vestibular signal. The intensity of the signal is indicated by the associated eye movement or nystagmus. Robert Barany received the 1914 Nobel Prize in medicine for describing the endolymphatic flow that causes cupular deflection during the caloric test in terms of a buoyancy-driven natural convective mechanism driven by the thermal irrigation [1]. Microgravity caloric tests aboard the 1983 SpaceLab1 mission produced nystagmus with an intensity comparable to those elicited during post- and pre-flight tests on earth [2], thus contradicting the basic premise of Barany's convection hypothesis and pointing out that the physics of the vestibular apparatus needs to be more precisely deciphered.

The first mathematical description of semicircular canal macromechanics is credited to Wilhelm Steinhausen [3] who formulated a classical torsion-pendulum model for the dynamic behavior. This analogy viewed the loop of endolymph as providing rotational inertia, the cupula as invoking the restoring stiffness, and the viscosity of the endolymph as supplying the viscous drag. As a result, the torsion pendulum model is essentially a band-pass filter relating the displacement of the cupula to the angular velocity of the head. The first work, which seriously focused on the fluid dynamics of the semicircular canals, is due to Van Buskirk et al. [4]. They assumed the endolymph to be an incompressible Newtonian fluid and accounted for the effect of the utricle and cupula through their contributions to the overall pressure gradient term. The fluid dynamics of the caloric test was first examined by Steer [5] and then by Young [6]. They used a lumped model of the endolymph loop to evaluate the pressure difference across the cupula during the thermal stimulation and relate that to the experimentally measured nystagmus behavior. Later Damiano [7] developed a continuum model describing the macromechanics of the caloric stimulation. He exploited the slender torroidal geometry of the canal and used perturbation analysis to study the dynamic response of the canal system to a singular harmonic thermal line source applied directly to the semicircular duct wall.

In this paper, we will present a comprehensive FSI model for the lateral semicircular canal (LSCC) system outside the restrictive confines of a lumped system approach or perturbation analysis and for the first time using a finite element numerical model, we will rigorously examine the details of the dynamic coupling between the endolymphatic flow in the canal and the structural deformation of the cupula partition during the caloric test.

2. Mathematical formulation

A two-dimensional cross section of the LSCC is presented in Fig. 1(a). The geometry and all the associated dimensions are extracted from measured human data by Curthoys and Oman [8]. The canal system consists of three main regions: the semicircular duct, the ampulla and utricle cavities. The ampulla cavity is the widened area of the canal at one end just before it communicates with the utricle. A crest like septum called crista transverses the ampulla perpendicular to the longitudinal axis of the canal. The cupula extends from the surface of the crista to the ceiling of the ampulla as shown in Fig. 1 forming what appears to be a watertight seal. The caloric test is usually performed with the patient in supine position and the head tilted 30° up placing the horizontal canal in the vertical plane aligned with the gravitational field. Thus the endolymphatic flow generated by the caloric irrigation is driven by two mechanisms: natural convection due to the gravitational body force and expansive convection due to the thermal expansion of the endolymph.

In order to formulate the governing equations of motion and energy conservation for the cupula–endolymph system, an Arbitrary Lagrangian Eulerian (ALE) approach is adopted. Fluid flow in the semicircular canal system is described in terms of the two dimensional Navier–Stokes equation:

$$\frac{\partial \rho}{\partial t} + \vec{\nabla} \cdot (\rho \vec{u}) = 0 \tag{1}$$

$$\rho_o \frac{\partial \vec{u}}{\partial t} + \rho_o (\vec{u} - \vec{u}_m) \vec{\nabla} \cdot \vec{u} = -\vec{\nabla} p + \mu \nabla^2 \vec{u} + \rho \vec{g} \tag{2}$$

where density is given by

$$\rho = \rho_o [1 + \beta_T (T - T_o)] \tag{3}$$

The energy equation can be written as:

$$\rho_o c \frac{\partial T}{\partial t} + \rho_o c (\vec{u} - \vec{u}_m) \vec{\nabla} \cdot T = k \nabla^2 T \tag{4}$$

Here, ρ, $\vec{u}$, p, and T, are respectively the density, velocity, pressure and temperature. Time is denoted by t and μ, β_T, c, k, are respectively the dynamic viscosity, thermal expansion coefficient, heat capacity, and thermal conductivity of the fluid. The gravitational acceleration is represented by $\vec{g}$ and subscripts o and m refer to reference and mesh values respectively.

According to the Eqs. (1)–(4) the endolymph is assumed to be a Newtonian weakly compressible fluid with constant properties except for density that is a linear function of the temperature but not pressure. The values for the endolymph conductivity, volume expansion coefficient, reference density, and viscosity are taken from measured data provided by Steer [9] and its specific heat was assumed to be equal to water. Because of the

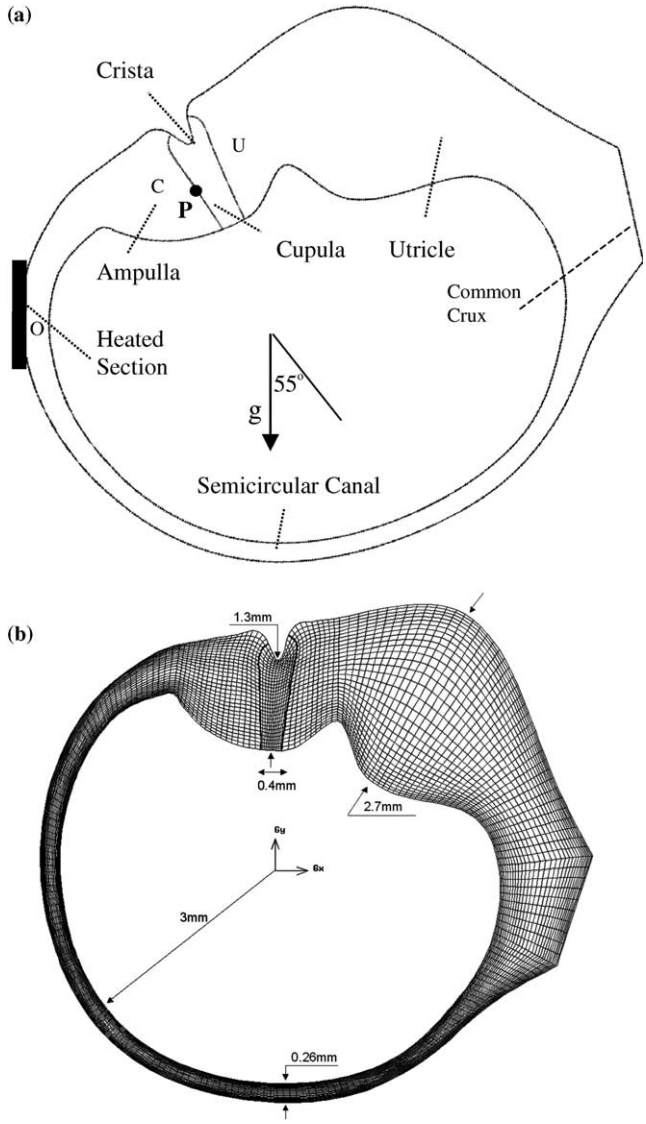

Fig. 1. (a) A Cross-Sectional View of The LSCC in The Optimum Supine Orientation; (b) Finite Element Mesh used for The FSI Simulations.

temperature dependence of density, there is a tight coupling between the energy and Navier–Stokes equations through the density term in the continuity equation and the buoyancy term in the momentum equation.

Non-slip stationary boundary conditions are applied at all the physical boundaries of the canal except for the wetted surfaces of the cupula, where the velocity is specified through the coupling with the structural equations, and at the outlet to the common crux, where the nodal velocities are left free to accommodate inflow and outflow of endolymph between the LSCC and the other canals. All the boundaries of the canal system are assumed to be at the body temperature, namely 37 °C, which is also the reference temperature, T_0. At time zero, an instantaneous temperature rise or fall is imposed on a segment of the canal as shown in Fig. 1.

Once the endolymph is brought into motion due to either natural or expansive convection or both, it produces a pressure differential across the cupula causing it to bend. The Navier equation of motion for the cupula can be written in terms of the displacement vector, $\vec{d}$, as

$$\rho_c \frac{\partial^2 \vec{d}}{\partial t^2} = \vec{\nabla} \cdot \boldsymbol{\sigma} + \rho_c \vec{g} \tag{5}$$

Following the incremental Updated Lagrangian approach and through application of principal of virtual

displacement and Gauss's theorem, a weak form of Eq. (5) is derived as:

$$\int_{V(t)} \rho \delta \vec{d}\, \frac{\partial^2 \vec{d}}{\partial t^2}\, \mathrm{d}V + \int_{V(t)} \mathbf{S}\boldsymbol{\delta}\mathbf{E}\, \mathrm{d}V = \int_{V(t)} \rho\, \vec{g}\, \delta \vec{d}\, \mathrm{d}V + \int_{A_\sigma(t)} \vec{t}\, \delta \vec{d}\, \mathrm{d}A \tag{6}$$

Here **S** and **E** are the second Piola–Kirchhoff stress and Green strain tensors respectively. The virtual work displacement vector, the traction force, and the Cauchy stress tensor are represented by $\delta \vec{d}$, $\vec{t}$, and $\boldsymbol{\sigma}$ respectively. Finally, V and A depict volume and area, while subscripts c and e refer to the solid and endolymph, respectively. The relationship between the stress and strain tensors can be expressed in a generalized form such as

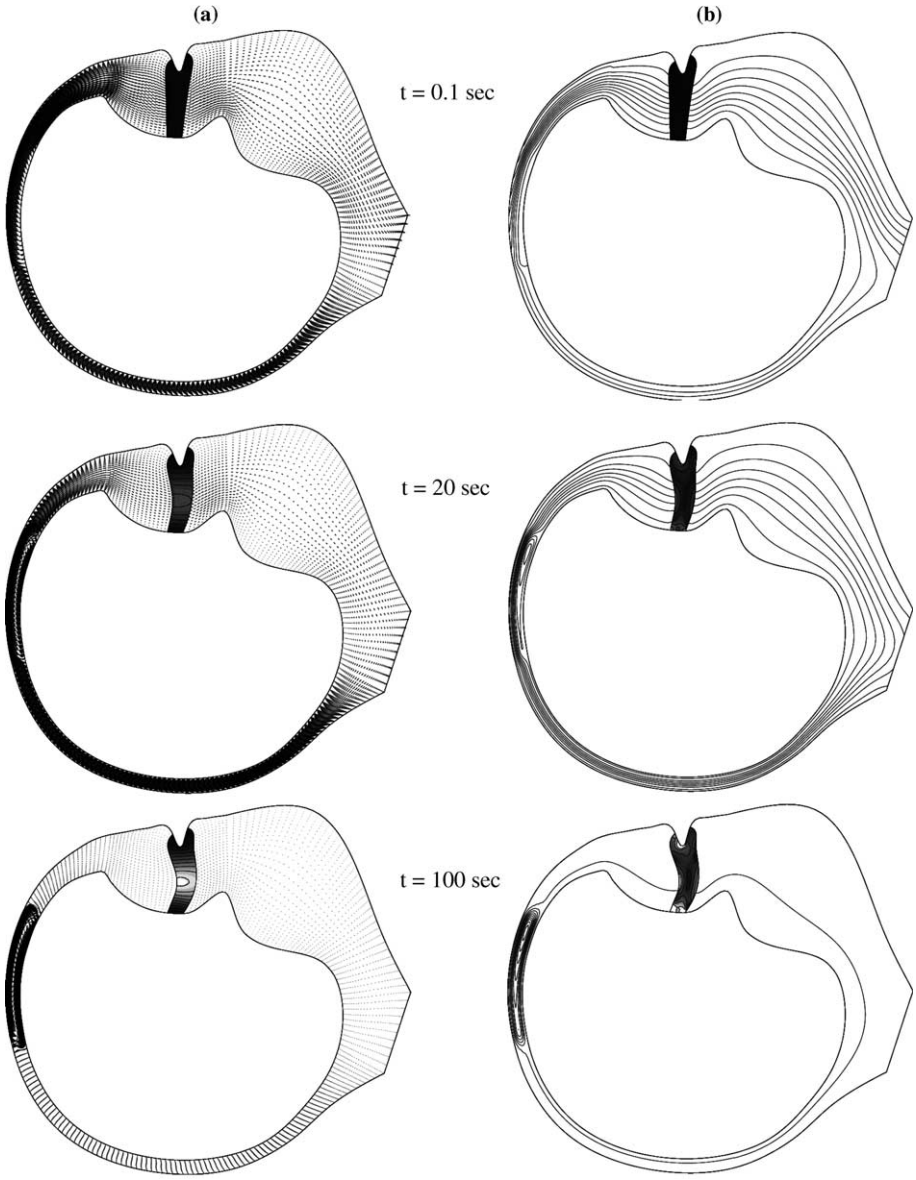

Fig. 2. Time Sequences of The Endolymph Velocity and Cupula Displacement Fields (a) and The Endolymph Streamline and Cupula Stress Fields (b) during a Hot Supine Caloric Test with $\Delta T = 7\,^{\circ}\mathrm{C}$. Maximum Velocity: $0.60(10)^{-2}$ cm/s at $t = 0.1$ s; $0.38(10)^{-2}$ cm/s at $t = 20$ s; and $0.28(10)^{-2}$ cm/s at $t = 100$ s. Displacement: Maximum Value=$0.194(10)^{-1}$ cm; Contours from 0.02 cm (Black) to -0.002 cm (White). Stress: Maximum Value=8.6 dynes/cm^2; Contours from 1 cm (Black) to 0 dynes/cm^2 (White).

$$\mathbf{S} = \mathbf{DE} \tag{7}$$

For a 2D plane stress case and assuming that the cupula is a linearly elastic material undergoing large deformation involving small strains, the elasticity tensor **D** can be defined in terms of the Young's Modulus, E, and Poisson ratio, v, of the solid as:

$$\mathbf{D} = \begin{pmatrix} 1 & v & 0 \\ v & 1 & 0 \\ 0 & 0 & \frac{1-v}{2} \end{pmatrix} \frac{E}{1-v^2} \tag{8}$$

The structural properties of the cupula are taken from Damiano [7]. Its Poisson Ratio was set to be 0.48, appropriate for a nearly incompressible membrane and its Young's Modulus was varied parametrically between 5–100 dynes/cm^2 with 5 dynes/cm^2 used as the base value.

Heat transfer through the cupula is governed by an energy conservation equation similar to Eq. (4) for the fluid. The conductivity, density, and specific heat of the cupula were assumed to be the same as the endolymph.

The movement of cupula is restricted at the top and bottom of its cross-section where a tight seal is formed with the ampulla wall. Cupula displacements at these two boundaries are set to zero. The strong coupling between the fluid flow and the structural deformations is rigorously preserved through a balance of traction forces and continuity of velocities and displacements at the wetted surfaces of the endolymph–cupula boundaries and can be summarized as follows:

$$d_e = d_c \tag{10}$$

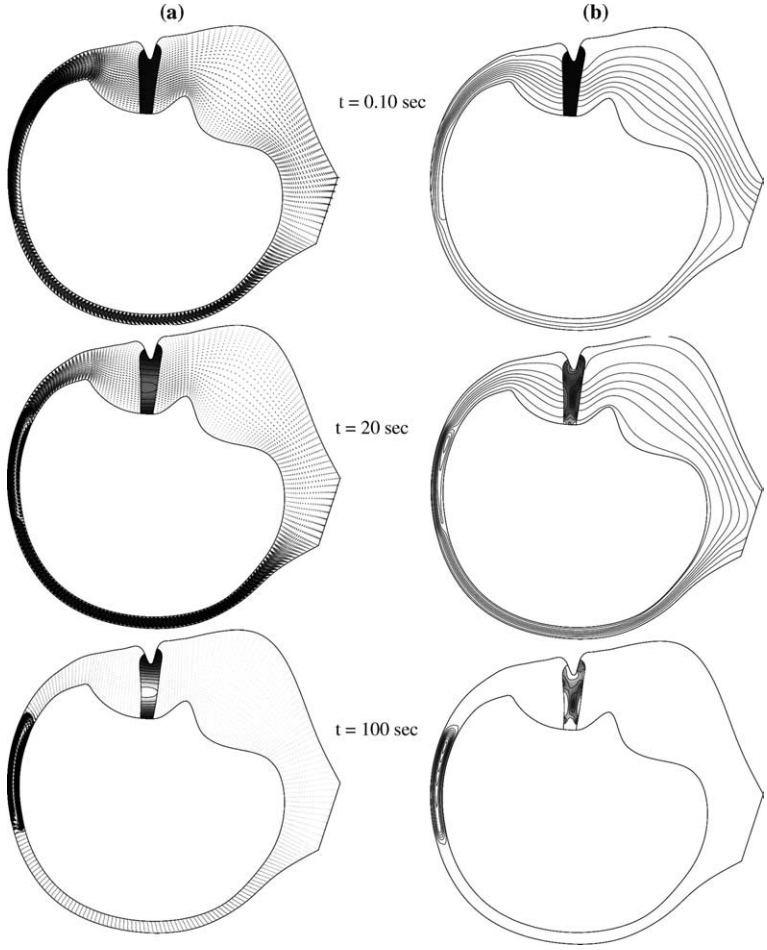

Fig. 3. Time Sequences of The Endolymph Velocity and Cupula Displacement Fields (a) and The Endolymph Streamline and Cupula Stress Fields (b) during a Hot Supine Caloric Test with $\Delta T = 1\,^{\circ}\mathrm{C}$. Maximum Velocity: $0.85(10)^{-3}$ cm/s at $t = 0.1$ s; $0.54(10)^{-3}$ cm/s at $t = 20$ s; and $0.39(10)^{-3}$ cm/s at $t = 100$ s. Displacement: Maximum Value=$0.278(10)^{-2}$ cm; Contours from 0.0028 cm (Black) to -0.00028 cm (White). Stress: Maximum Value=0.64 dynes/cm^2; Contours from 0.1 cm (Black) to 0 dynes/cm^2 (White).

$$\vec{u}_e = \frac{\partial \vec{d}_c}{\partial t} \tag{11}$$

$$\hat{n}_e \cdot \vec{t}_e = \hat{n}_c \cdot \vec{t}_c \tag{12}$$

3. Numerical methodology

FSI problems have drawn considerable attention in many areas of engineering and science in recent years. As a result, an impressive array of numerical capabilities to deal with FSI have been developed and widely used in academia and industry [10,11]. In the present work, numerical solutions of the governing system of coupled nonlinear partial differential equations are generated using a customized in-house version of the finite element code Fidap. Transient solutions are generated using the implicit backward Euler time integration scheme for the flow equations and the second order Bossak integration scheme for the structural equation. At each time step (loop) the computational fluid dynamics and computational structural dynamics counterparts of the problem are solved together following the ALE approach based on a moving mesh which deforms according to the pseudo-elastic body displacements at the cupula-endolymph surfaces. The strong coupling between the fluid flow and the structural deformations is rigorously preserved through the balance of the traction forces and the imposition of transfer-compatibility conditions for velocity and displacement at the wetted surfaces. An iterative segregated solution methodology is implemented that can be briefly summarized as follows:

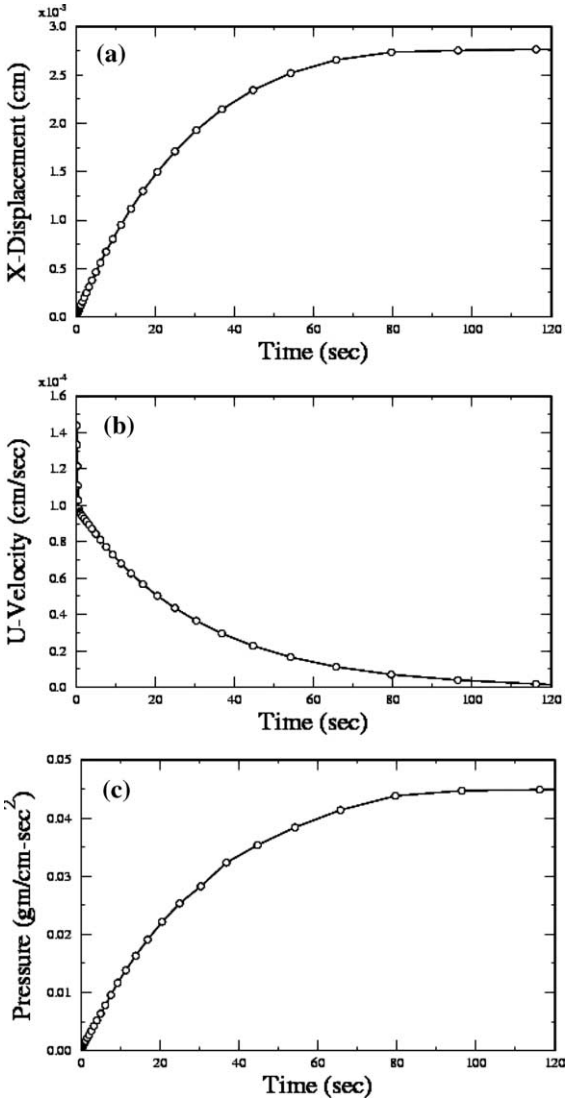

Fig. 4. Time Histories of Cupula Displacement (a), Cupula Velocity (b), and Transcupular Pressure Difference (c) for a Hot Supine Caloric Test with $\Delta T = 1\,^{\circ}C$.

CFD: Initial conditions for the velocity and temperature variables, boundary conditions at the non-wetted surfaces, and transfer-compatibility conditions at the wetted surfaces are imposed. The fluid velocity and pressure and temperature fields are solved for using a segregated scheme. The traction force vectors at the wetted surfaces are calculated.

CSD: The external loads and fluid traction forces are applied and the initial and boundary conditions for the equation of motion of the solid are imposed. Eq. (6) is integrated to yield the structural displacement, velocity and acceleration vectors. The displacements at the wetted surfaces are calculated and the surface nodal locations are adjusted accordingly.

CMD: The ALE mesh is solved for according to the pseudo-elastic body displacements at the wetted surfaces and using predesignated and optimized dynamic mesh parameter. The mesh geometry is updated and the mesh velocity field is calculated for input to the CFD loop.

The solutions presented in this paper were generated on a nonuniform mesh with 6374 quadratic elements as shown in Fig. 1(b). At each time step, a convergence tolerance of 0.0001 was used for the velocity and displacement norms and a convergence tolerance of 0.001 was used for the fluid–solid surface norm. All solutions were started with the entire domain at a uniform body temperature and zero velocity, displacement, and stress fields and terminated when steady state conditions were reached. Values for the mesh elasticity and Poisson ratio were chosen to be 1 dynes/cm^2 and .001, respectively. Comprehensive grid and time-step convergence tests were performed to ensure spatial and temporal resolution of the generated solutions.

4. Results and discussion

During the caloric test, the ear canal is usually irrigated with water at around 44 °C. Cawthrone and Cobb [12] have experimentally shown that this irrigation temperature produces a temperature rise of about 1 °C in the region of the horizontal canal closest to the temporal bone. Therefore, for the base case simulations presented here, it is assumed that all the boundaries of the canal system are at the body temperature, namely 37 °C, and at time zero, a 1 °C temperature rise is imposed on a section of the canal as indicated in Fig. 1. This thermal impulse is maintained throughout the transient simulation until steady state conditions are reached.

The evolution of the endolymphatic flow and its impact on the the cupular displacement and stress fields during a *hot* caloric test are depicted in the time sequences of Figs. 2 and 3 for imposed temperature increases of 7 °C and 1 °C, respectively. Although the 7 °C temperature rise represents the maximum attainable temperature increase, it is unrealistic as the results of Cawthrone and Cobb [12] suggest. This case has been included here only because it results in a strong endolymphatic and a large cupular displacement that can be easily discerned by a naked eye. At $t = 0.1$ secs, the temperature boundary layer has almost fully penetrated the duct. Consequently, an endolymphatic flow ensues that is driven almost equally by buoyant and expansive convection. At this instance the cupula is still in its unstressed and undeformed state as indicated in Fig. 2 and 3. At $t = 20$ s, the clockwise recirculating flow due to the buoyancy-driven natural convection becomes more pronounced, especially, in the vicinity of the heated-section creating a negative pressure gradient across the cupula. This fluid loading causes slight bending of the membrane as evident from the displacement fields of Fig. 2(b) and Fig. 3(b) and creates stress concentrations in the regions around the crista, along the lower ampulla wall, and near the region of maximum cupular displacement close to the vertical center of the membrane as shown in Fig. 2(b) and Fig. 3(b). At $t = 100$ s, steady-state conditions are reached whereupon the expansive convection has almost completely dissipated itself and a relatively strong natural convection vortex has emerged as the dominant endolymphatic flow mechanism in the canal. It is interesting to note that the model predicts a bulging or bending of the cupula towards the utricle in accordance with the experimental observations for a *hot* caloric stimulation. This is due to the negative pressure gradient imparted across the cupula by the clockwise recirculating vortex. Although, the ensuing natural convective flow is recirculating, this situation is sometimes erroneously referred to in the literature as an *ampullopetal* flow as if the endolymph flow was moving towards the ampula/cupula.

Fig. 4 contains the time histories for displacement, velocity, and pressure of a point (P) on the cupula surface (see Fig. 1) for the $\Delta T = 1$ °C case. The highest cupula velocities occur at the initiation of the test as evident from Fig. 4(b) and are due to the impact of the rapid expansive flow. But the expansive velocity diminishes quite fast and thus contributes very little to the overall displacement of the cupula that reaches a plateau in about 80 s as seen in Fig. 4(a). Thus most of the cupula displacement is due to the natural convective flow that takes over from early on, marked by a sudden change of slope in the velocity history of Fig. 4(b). Naturally,

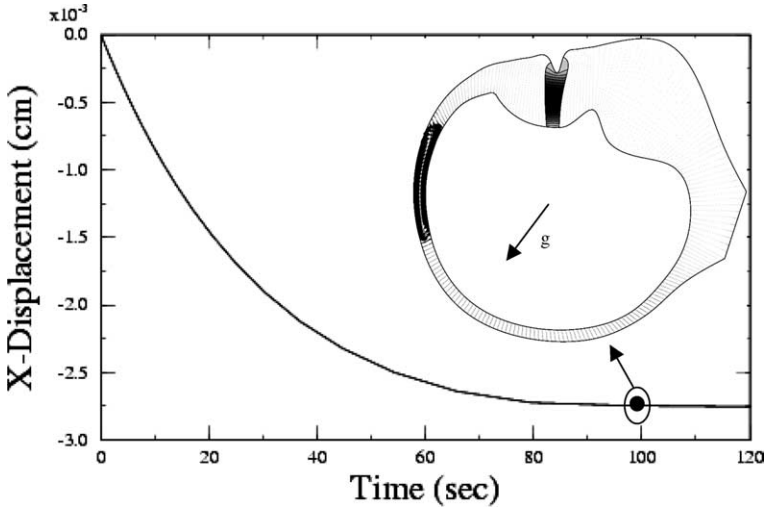

Fig. 5. Time History of Cupula Displacement for a Cold Supine Caloric Test with $\Delta T = -1$ °C.

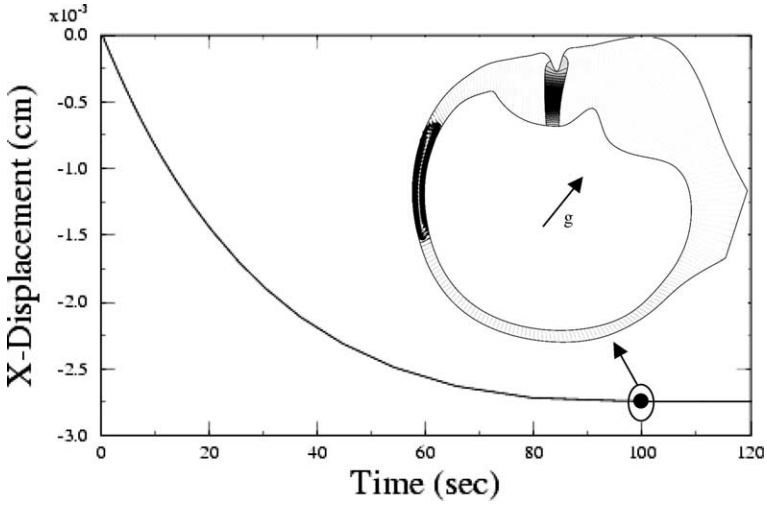

Fig. 6. Time History of Cupula Displacement for a Hot Prone Caloric Test with $\Delta T = 1\,^{\circ}\mathrm{C}$.

as a steady state recirculating flow condition is approached and the cupula displacement reaches a plateau, the cupula velocity goes to zero. The time evolution of the pressure drop across the cupula (along the line of maximum deflection) is presented in Fig. 4(c). It is interesting to note that there is a one-to-one correspondence between the transcupular pressure difference of Fig. 4(c) and the cupula displacement of Fig. 4(a).

Caloric experiments indicate that there is a reversal of nystagmus if a *cold* caloric test is performed in the *supine* position, or if the patient is oriented in the *prone* position during a *hot* caloric test. This is corroborated by the FSI simulations shown in Figs. 5 and 6 for the cold/prone and a hot/supine caloric test conditions. Both of these cases, result in a counterclockwise natural convective flows (as shown in the insets of Figs. 5 and 6) that produce a positive pressure difference across the cupula resulting in a bending or bulging of the partition towards the canal side of the ampulla. This situation is referred to, again incorrectly, as the *ampullofugal* flow denoting an endolymph that flows away from the cupula and towards the canal.

The extent of cupular deflection is controlled by two important factors. First is the imposed temperature rise (or the irrigation temperature) that controls the intensity of the endolymphatic flow. Second is the Young's Modulus of the cupula that determines the cupular structural response to the dynamic fluid loading. Our results indi-

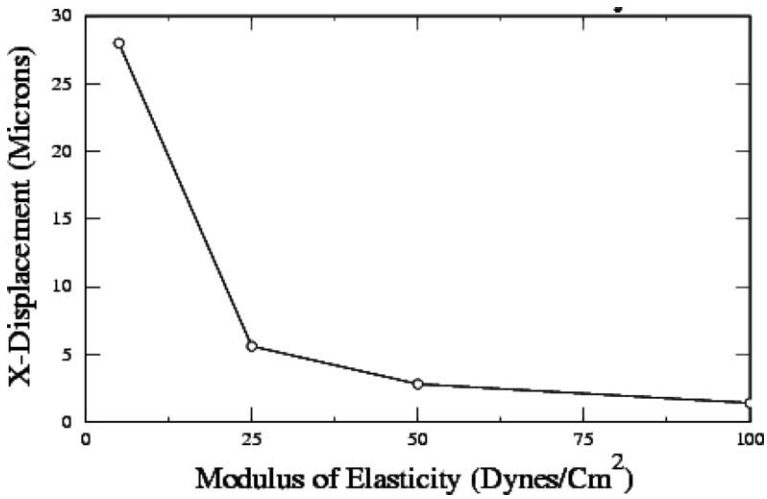

Fig. 7. Effect of the Young's Modulus of Elasticity of the Cupula on the Maximum Displacement.

cate that while the maximum cupula displacement during a caloric test varies linearly with the irrigation temperature, it has a nonlinear dependence on the Young's Modulus as demonstrated in Fig. 7. This relationship can be best described by a power law and arises due to the boundary value problem that is inherently solved for the cupula geometry.

5. Conclusion

In this paper we presented a finite element FSI model for the LSCC system with a rigorous treatment of the coupling between the fluid flow and the structural dynamics counterparts. Transient simulations were used to reveal the details of the dynamic interaction between the endolymphatic flow driven by both natural and expansive convections and the structural deformation of the cupula during a typical caloric irrigation test. Numerical results are in qualitative agreement with experimental and clinic observations of the nystagmus directions for hot-supine, cold-supine and hot-prone test conditions. Parametric simulations also indicate that the maximum displacement of the cupula is a strong function of its structural properties. Therefore, a more elaborate and realistic material model for the cupula, which is a hydrated fiber-reinforced gel-like structure, is deemed necessary and will be developed in future.

Acknowledgment

This work was supported by the Microgravity Research Division at NASA Glenn Research Center (GRC). Computational and system-related support and resources provided by the Computational Microgravity Laboratory at NASA GRC and the Ohio Supercomputer Center (OSC) are also gratefully acknowledged.

References

[1] Barany R. Untersuchungen uber den vom Vestibularapparat des Obres reflektorisch ausgelosten rhytmischen Nystagmus und seine Begleitertscheinungen. Monatsschr Ohrenheilkd 1906;40:193–297.
[2] Scherer H, Brandt U, Clarke A, et al. European Vestibular Experiments on Spacelab-1 Mission: 3. Caloric Nystagmus in Microgravity. Exp Brain Res 1980;64:255–63.
[3] SteinHausen W. Uber die Beobachtung der Cupula in den Bogengangsampullen des Labyrinths des Lebenden Hechts, Pflugers Arch. Ges Physiol, 1933; 23: 500-512.
[4] Van Burskirk WC, Watts RG, Liu YK. The Fluid Mechanics of The Semicircular Canals. J Fluids Mechanics 1976;78(1):87–98.
[5] Steer RW. Influence of Angular and Linear Acceleration and Thermal Stimulation on the Human Semicircular Canal. PhD Thesis, MIT, Cambridge, MA, 1967.
[6] Young JH. Analysis of Vestibular System Responses to Thermal Gradients Induced in the Temporal Bone. PhD Dissertation, University of Michigan, Ann Arbor, Michigan, 1972.
[7] Damiano ER. Continuum Models of Rotational and Caloric Stimulation of The Vestibular Semicircular Canal. PhD Dissertation, Rensselaer Polytechnic Institute, Troy, New York, 1993.
[8] Curthoys IS, Oman CM. Dimensions of the Horizontal Semicircular Duct, Ampulla and Utricle in Human. Acta Otolaryngol (Stockh) 1987;103:254–61.
[9] Steer RW, Li YT, Young LR, Meiry JL. Physical Properties of the Labyrinthine Fluids and Quantification of Phenomena of Caloric Stimulation, Third Symposium on the Role of Vestibular Organs in Space Exploration, 1967; NASA SP-152; pp. 409–512.
[10] Bathe KJ, Zhang H, Ji S. Finite Element Analysis of Fluid Flows Fully Coupled with Structural Interactions. Comput Struct 1999;72(1–3):1–16.
[11] Rugonyi S, Bathe KJ. On Finite Element Analysis of Fluid Flows Fully Coupled with Structural Interactions. Comput Modeling in Engineering & Sciences 2001;2:195–212.
[12] Cawthorne TE, Cobb WA. Temperature Changes in The Perilymph Space in Response to Caloric Stimulation in Man. Acta Otolaryngol 1954;44:580–8.